transformation of an electromagnetic (EM) field between micro- and macroscopic systems, which will open up a new field of off-shell science.

This fiber probe has been used at the heart of a novel microscope and spectrometer that exhibit ultrahigh spatial resolution beyond the diffraction limit of propagating light [3]. Conformations and structures of a variety of nanometric materials have been measured and analyzed with these instruments, which have been commercially available [4].

## 2. Experimental evaluation of the dressed photons

In order to identify requirements from an experimental viewpoint, this section reviews the principles of creation and measurement of DPs. The structures and performance levels of fiber probes are also reviewed. Also, it is pointed out that a fiber probe can be replaced by a nano-particle (NP). Finally, requirements for developing novel theories are presented.

## 2.1 Principles of creation and measurement of dressed photons

As schematically explained by Fig. 1, the DP is a quantum field that exists in an off-shell area that is displaced from the shell of the dispersion relation between energy and momentum [1,5]. Since the uncertainty $\delta p$ of the momentum $p$ is large in this area $\left( \delta p \gg p \right)$, the size $a$ of the DP is much smaller than the wavelength $\lambda$ of the propagating light $\left( a \ll \lambda \right)$ due to the Heisenberg uncertainty principle. In order to create such a small DP, a fiber probe has been used, as is schematically explained by Fig. 2(a). The operating mode of the fiber probe in this figure is called the illumination mode (I-mode) [6], in which the tail of the fiber probe is illuminated with propagating light (the EM field on shell) to create a DP at the nanometric tip of the probe.

Since the created DP is localized on the tip, it is measured by inserting a sonde into the DP for acquiring the response from the DP. That is, the DP is measured by acquiring its response to a stimulus applied from the outer system. A nano-particle (NP) has been used as such a sonde (Fig. 2(b)). By putting this NP in close proximity to the tip of the fiber probe, the DP energy is exchanged between the fiber probe tip and the NP, resulting in excitation of an electron in the NP. The excited electron can create a photon. Since this photon is a conventional scattered light field on shell, it can be

2

measured by a conventional photo-detecting device, and thus, the response can be acquired. In this I-mode, the fiber probe and NP respectively play the roles of a light source and a detector for creating and measuring the DP.
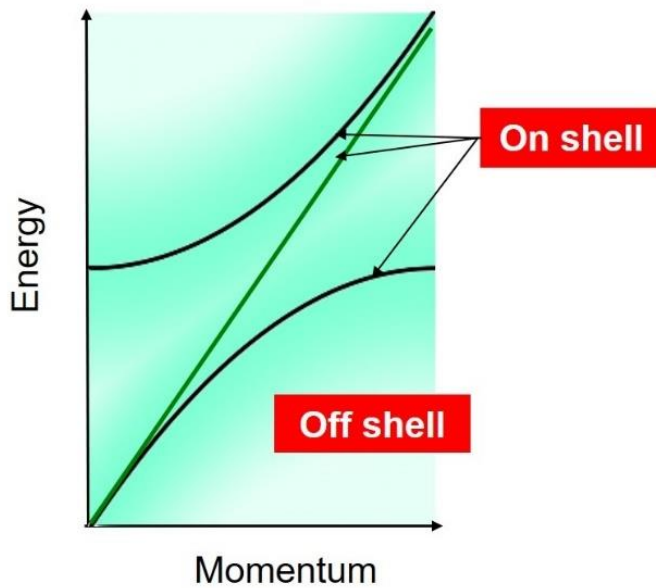


Fig.1    Dispersion relation between the momentum and energy of the electromagnetic field. The green line and black curves are for the fields in vacuum and in a macroscopic material, respectively. They are the fields on shell. The green shaded rectangle is for the field off shell.

It is possible to exchange the roles of the fiber probe and the NP: First, the NP is illuminated by propagating light to create the DP. Next, a fiber probe, which is used as a sonde, is brought close to the NP (Fig. 3(b)). The DP energy is thus exchanged between the NP and fiber probe tip, resulting in excitation of an electron in the tip of the fiber probe. The excited electron can create a photon, i.e., scattered light. Since this scattered light is guided through the fiber probe and reaches its tail, it can be measured by a conventional photo-detecting device, and thus, the response can be acquired. The operating mode of the fiber probe in this figure is named the collection mode (C-mode) [6].
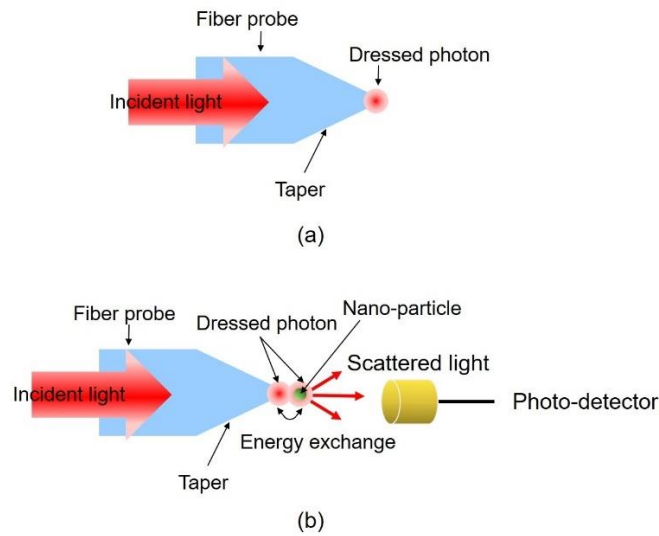
Fig.2　Illumination mode for the fiber probe operation.

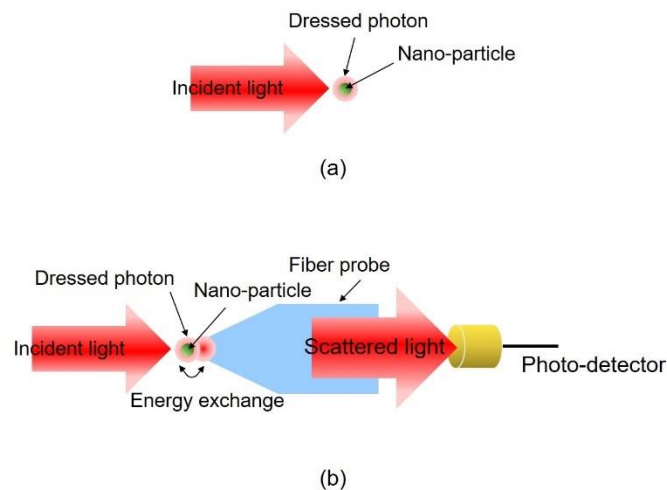(a) For creating the DP. (b) For measuring the DP.



Fig.3　Collection mode of the fiber probe operation.

(a) For creating the DP. (b) For measuring the DP.

## 2.2 Performance of fiber probes

As is summarized in Fig. 4(a), a variety of fiber probes have been developed so far, some of which have been commercially available [2]. The size and conformation of the tip and taper of the fiber probe have been empirically controlled during the fabrication process, resulting in sufficiently high efficiencies for creating and measuring DPs for practical use. These high efficiencies are indispensable for reliable conversion of the EM field

from macro- to microscopic systems and also from micro- to macroscopic systems, respectively, in the case of the I- and C-modes.
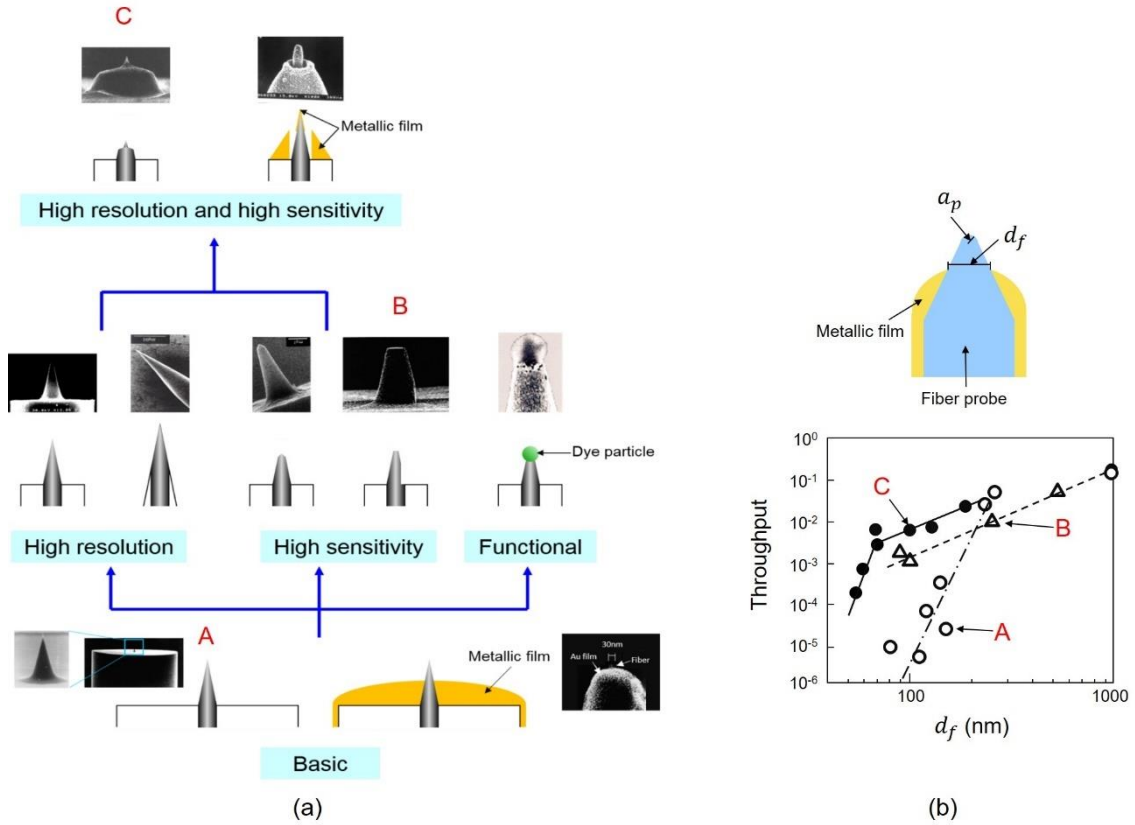


Fig. 4   Developed fiber probes.

(a) Cross-sectional profiles and scanning electron microscopic images. (b) The efficiency of measuring the DP. $d_f$ is the foot diameter of the taper protruding from an opaque metallic film. Open circles, open triangles, and closed circles represent the experimental results measured for the fiber probes A, B, and C in (a), respectively.

Figure 4(b) represents the efficiency of measuring the DP acquired when the fiber probe was used in the I-mode [7]. This efficiency is expressed as the "throughput", which is the ratio between the measured optical power and the optical power incident at the tail of the fiber probe. The horizontal axis is the diameter $d_f$ of the foot of the taper protruding from an opaque metallic film, which was deposited for blocking unwanted scattered light. In these old experimental results acquired more than 15 years ago, it should be pointed out that a certain amount of unwanted scattered photons was

measured simultaneously with the DP when $d_f$ was larger than 100 nm. This signal mixing was due to insufficient shielding resulting from the immature metallic film coating technology available at the time.

It should be noted that the spatial resolution of this novel microscope and spectrometer are determined by the value of the tip radius, $a_p$. Detailed discussions of the special resolution, and also of the image contrast, are given in Appendix [8].

## 2.3 Using nano-particles

A novel method has been developed recently in order to replace the role of the fiber probe operating in the I-mode by an NP, as is schematically explained by Fig. 5(a). In this scheme, an NP is illuminated by propagating light to create a DP. One may worry that the creation efficiency will be very low because the interface between the macro- and microscopic systems, i.e., the taper of the fiber probe in Fig. 2, is missing in this configuration. However, novel interface devices, such as an optical nano-fountain and an optical energy transmitter [9], have been developed by using multiple NPs, enabling drastic increases in efficiency.
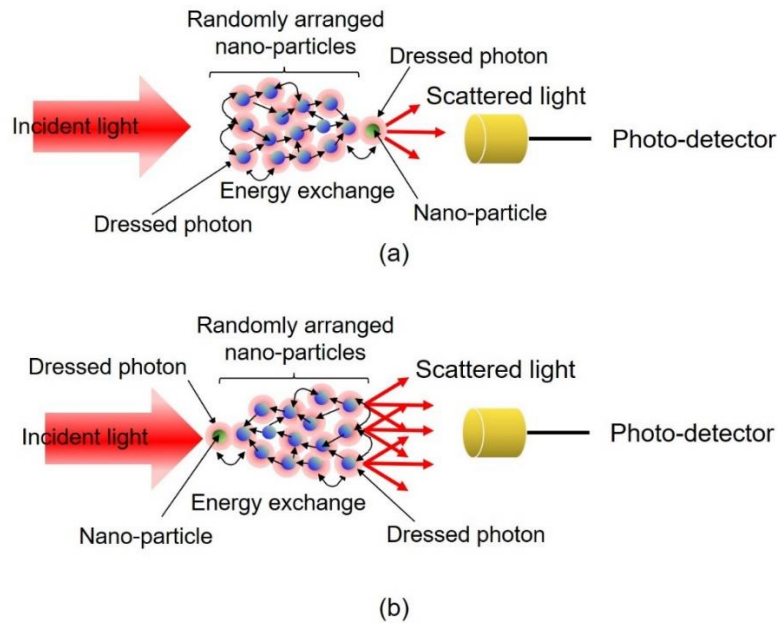


Fig. 5    Nano-particles for creation and measurement of the DP.

The multiple randomly arranged NPs correspond to the taper of the fiber probe.(a) For creating the DP. (b) For measuring the DP.

The replacement mentioned above has been realized also for the C-mode: As is schematically explained by Fig. 5(b), in this scheme, multiple NPs are arranged around the NP on which the DP is originally created. As a result, the DP energy is exchanged between the center NP and the surrounding multiple NPs to excite an electron. The excited electron can subsequently create scattered light, which can be acquired by a conventional photo-detecting device.

It should be pointed out that a specific phenomenon of autonomous DP energy exchange has been observed among multiple randomly arranged NPs [9]. That is, it has been experimentally confirmed that the optimum route was autonomously selected for the DP energy transfer in the optical nano-fountain and optical energy transmitter devices above.

## 2.4 Requirements for novel theories

The gray cone in the phase diagram of Fig. 6 represents the area in which the DP measuring efficiency is high, which was empirically found through experimental work on fabricating and using an I-mode fiber probe. Here, $a_p$ is the tip radius, $a_s$ is the radius of the spherical NP, $a_s / a_p$ is their ratio, and $e$ is the cone angle of the taper.

It should be pointed out that the efficiency is the highest when $a_s / a_p \sim 1$, which is due to the size-dependent resonance feature of the DP energy exchange [10]. A similar conical area can be derived also for the C-mode. A novel theory is required since one of the major requests from experimentalists is to find the optimum condition for realizing the highest efficiency of creation and measurement of DPs. It is expected that Fig. 6 will serve as a reference to find this condition.

To find the optimum condition, it should be also noted that the detailed profile of the tip and taper of the fiber probe are not smooth but have some roughness on their surfaces, as is schematically shown in Fig. 7. Specifically, Fig. 7(a) represents a conical surface profile with a smooth surface, which can be observed from a far field view point. However, the NP in Fig. 2(b), which is installed in the near field of the fiber probe surface, may see a magnified surface and find a lot of bumps (Fig. 7(b)), on which multiple DPs with a variety of sizes are created. That is, a hierarchy exists in the DP measurement, which depends on the position and size of the NP to be used as a sonde for the measurement. A novel theory that can describe this hierarchy, as well as the
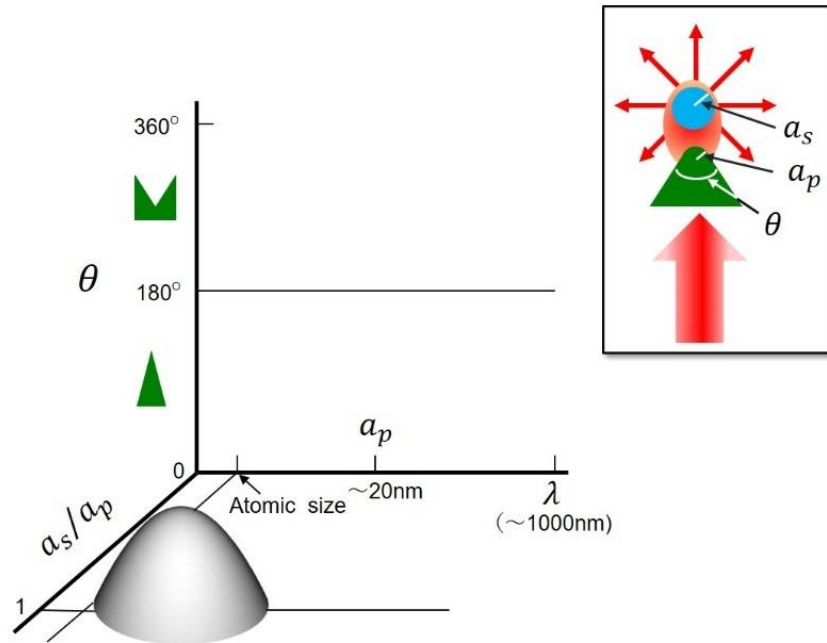
autonomy mentioned in Section 2.3, is needed.



Fig. 6　Phase diagram for representing the area in which the efficiency of measuring the DP is high. ` is the wavelength of the light incident on the fiber probe.
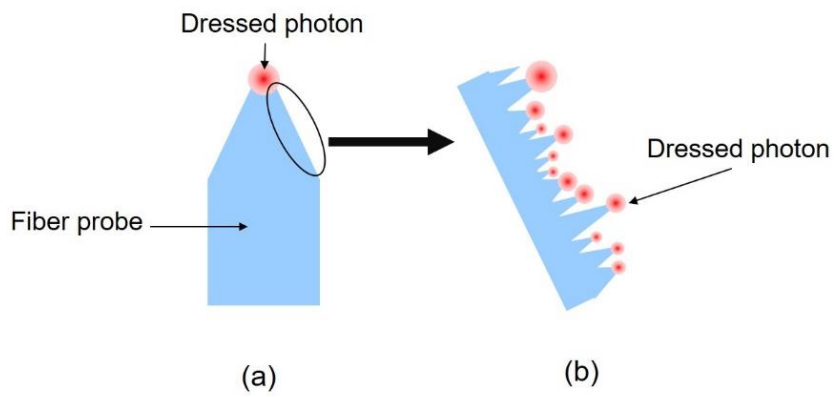


(a)　　　　　　　　　　　(b)

Fig. 7　Hierarchy of measuring the DP created on the tip and taper of the fiber probe.
(a) Cross-sectional profile of the tip and taper of the fiber probe.(b) Magnified profile of (a).

## 3 Strategies for novel theories

This section presents problems to be solved, which have been requested by experimentalists. Some promising novel theoretical methods for solving these problems are reviewed.

## 3.1 Problems to be solved

In the case where the I-mode is used by illuminating the tail of the fiber probe with propagating light, it is advantageous to create:

   (A) a small DP for achieving high-spatial-resolution measurement,

and

   (B) a high energy DP for achieving high-sensitivity measurement.

      In order to find the criteria for designing a fiber probe for creating these DPs, the following two-step theoretical calculation ought to be carried out (Fig. 8). That is, the problems to be solved are

(1) 1$^{st}$ step: Three kinds of EM fields in the taper have to be derived. They are

   a) Propagating light, which is guided through the taper (EM field on shell).

   b) Scattered light, which is dissipated via radiation from the taper (EM field on shell).

   c) A DP (EM field off shell), whose size is equivalent to the size of the taper because the spatial profile of the DP is expressed as a Yukawa function [10].

(2) 2$^{nd}$ step: The DP on the tip of the fiber probe has to be derived.
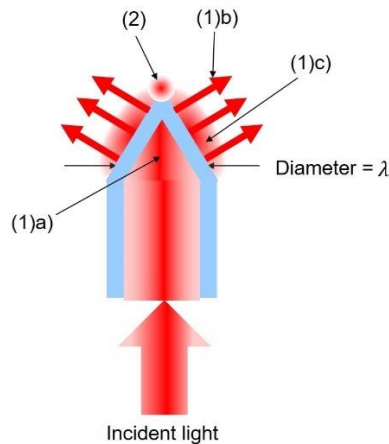


Fig. 8   Two-steps for theoretical calculation.

$\lambda$  is the wavelength of the light incident on the fiber probe.

      The DP in (2) is created as a result of the DP energy transfer from the fields (1a) and (1c). It means that the conformation and structure of the taper play essential roles in creating the DP of (A) and (B) on the tip. In other words, it is essential to optimize the magnitude of the energy dissipated from the taper, which is the magnitude of the energy of the field (1b).

      It should be pointed out that this taper is the interface between micro- and macroscopic systems (i.e., between the tip and the tail of the fiber probe), and thus, it

plays an essential role in the micro–macro duality. However, EM fields in the taper have never been correctly described by the conventional EM field theories because these theories cannot be applied to the taper due to its sub-wavelength diameter. Namely, a method of numerical analysis based on Maxwell's equations (for example, the Finite Difference Time Domain (FDTD) method) is not suitable for deriving the EM field of (1b) and (1c) [11]. In particular, in the case of (1c), the use of the FDTD method is useless because it does not take into account the longitudinal component of the electric field [12].

## 3.2 Expected theoretical methods

Several novel theoretical methods have been proposed to solve the problems presented in Section 3.1. This section reviews these methods.

Figure 6 shows that the highest efficiency was obtained in the case of $a_s / a_p \approx 1$, due to the size-dependent resonance in the DP energy exchange between the fiber probe and the NP [10]. This case corresponds to the case where the magnitude of the energy dissipation from the taper (the scattered light energy of (1b) in Section 3.1) takes the minimum. Therefore, in order to find the creation methods (A) and (B) in Section 3.1, it is essential to explore the conformation and size of the fiber probe which maximize the difference between the energy of the DP localized at the tip and the energy lost due to dissipation at the taper. For this exploration, Fig. 9(a) was derived, in which the value of $a_s / a_p$ in Fig. 6 was replaced by the magnitude of the energy loss $E_d$ (magnitude of the light energy scattered from the taper). It should be noted that this figure uses the energy dissipation rate $\eta_d \left( \equiv E_d / E_i \right)$, which is defined by the ratio between $E_d$ and the energy $E_i$ of the light incident on the tail of the fiber probe. For this replacement, a semi-quantitative relation between $a_s / a_p$ and $\eta_d$ was derived based on Fig. 2.6 of ref. [10], which is shown by Fig. 9(b).

Here, the problem is that the conventional EM field theories cannot be used to analyze the magnitude $E_d$ of energy dissipation because the taper is of sub-wavelength size. To solve this problem, it would be advantageous to use the concept of effective mass of the EM field instead of using the conventional method. This may enable estimation of the magnitude of the energy dissipation by assuming that the energy

dissipation takes place during the process of transforming the massless free photon on shell to the off-shell photon with a finite mass. The Clebsch dual field theory was developed for this estimation by noting the duality between the fields in the space-like and time-like areas in the Minkowski diagram [1,13].
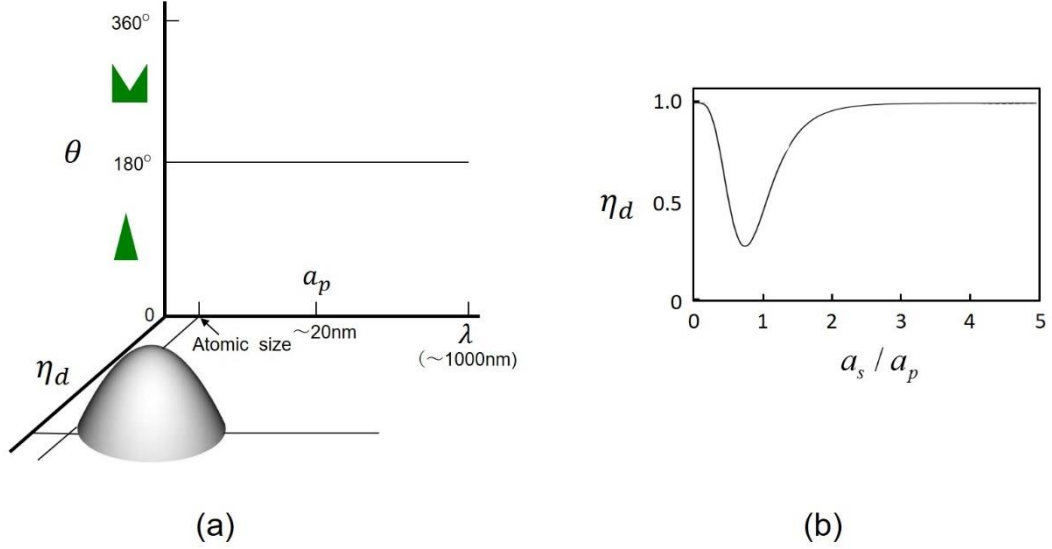


(a)                                                                 (b)

Fig.9    Phase diagram for representing the area in which the efficiency of measuring the DP is high.

(a) The ratio of the sizes $a_s / a_p$ in Fig. 6 is replaced by the energy dissipation rate $\eta_d$. (b) The relation between $a_s / a_p$ and $\eta_d$ used for illustrating (a).

The energy–momentum tensor of the Clebsch dual field is isomorphic to the left-hand side of the Einstein field equation represented as a Ricci curvature tensor defined in terms of a contracting Riemann tensor, thus suggesting an interpretation wherein the energy–momentum tensor of a virtual photon field carries a part of the energy–momentum of "vacuum", as in classical space-time. It also suggests that it may represent a so-far unidentified energy field similar to the controversial dark energy in cosmology, since, corresponding to its space-like characteristics, the associated scalar curvature is negative. According to a quantum mechanical point of view, a vacuum is considered as a fluctuating energy field where creation and annihilation of a variety of virtual particles occur incessantly.

Mathematical analysis of the Clebsch dual field shows that a space-like Clebsch field is stable as long as it exists in wave-like modes extending uniformly in space–time. However, once local perturbations arising from the interactions of material fields are

11

given, the energy of the Clebsch field becomes unstable and is transformed into a spatially localized form having a Yukawa-potential distribution if its energy level exceeds a certain threshold value. In the case of Figs. 2(a) and 3(a), the Yukawa-potential means that the spatial extent of the DP field corresponds to the sizes of the tip of the fiber probe and that of the NP, respectively. The above unstable Clebsch field consists of amplifying and damping fields. When we consider the latter, we can interpret it as a rapidly decreasing time-like mode returning the excited energy back to the environmental material field in a manner consistent with the conventional explanation given in terms of the uncertainty principle since the damping rate is proportional to the magnitude of the excited energy.

Based on the discussions above, applying the Minkowski diagram to the I-mode reveals that the EM fields in the light-like, time-like, and space-like domains correspond to the propagating light incident on the tail of the fiber probe, the scattered light radiating from the taper of the fiber, and the DP created on the tip of the fiber probe, respectively, as is schematically explained by Fig. 10(a). In the case of the C-mode, this correspondence is also explained by Fig. 10(b). Since the light-like field produces a pair consisting of time-like and space-like fields, the creation rate of the space-like field can be maximized by minimizing the creation rate of the time-like field. As a result, the DPs in (A) and (B) in Section 3.1 can be efficiently created. It should be pointed out that the hierarchy explained in Fig. 7 can be described by including the nonlinear interaction in the theoretical approach described above.
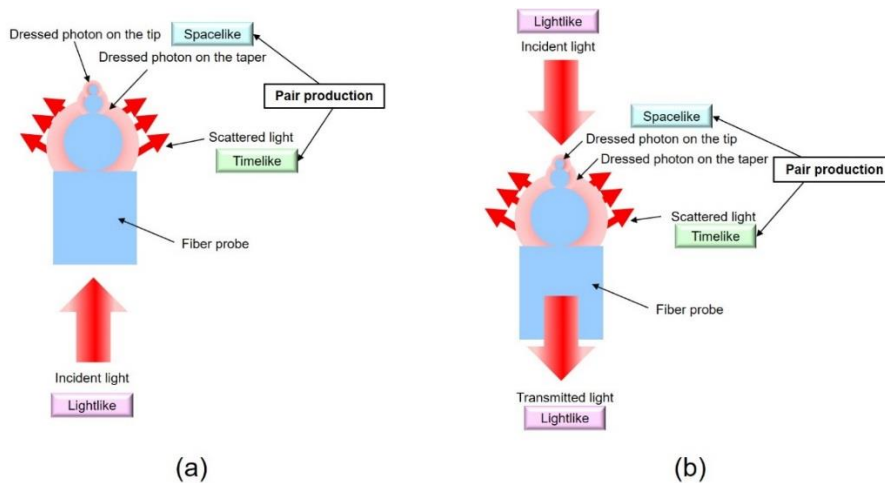


Fig.10　Electromagnetic fields in the light-like, time-like, and space-like domains.

(a) Illumination mode (transformation from macro- to microscopic systems). (b) Collection mode (transformation from micro- to macroscopic systems).

It should be noted that the gray cones in Figs. 6 and 9(a) have asymmetric profiles. This is because the DP is intrinsically created on the tip of the fiber probe, which has a translationally asymmetric profile. Theoretical models for the off-shell EM field should be developed based on this asymmetry. For this advanced theoretical model, use of the quadrality scheme [14] based on category theory is expected to be a promising approach for describing the transformation of the microscopic DP to the macroscopic system. Furthermore, a novel measurement theory should be constructed by noting that the fiber probe and NP in Figs. 2(b) and 3(b) form a composite system originating from the DP energy exchange. Tomita's decomposition theorem [15] is expected to be promising for this construction. Further advances in these theoretical studies are expected to lead to developments in the field of off-shell science.

## 4 Summary

This paper adopted a fiber probe to identify the requirements in theoretical studies for analyzing the physical properties of DPs. The principles of using this fiber probe in illumination and collection modes were reviewed. After the structures and performance of a variety of fiber probes were presented, it was pointed out that the fiber probe could be replaced by an NP, and that multiple NPs exhibited a specific phenomenon of autonomous energy transfer of the DP. A phase diagram was empirically derived through experiments in order to show the experimental condition for achieving high-efficiency measurements of the DP. Based on this diagram, requirements for a novel theory were identified to find the optimum condition giving the highest efficiency. Furthermore, it was required that this theory should be able to describe the intrinsic phenomena of the autonomy mentioned above, and also the hierarchy in the DP measurement.

It was pointed out that the conventional EM field theories cannot meet these requirements, as well as a description of the field in the taper of the fiber probe. To meet the requirements, some promising novel theoretical approaches were reviewed. One was an approach based on Clebsch dual field theory. The use of the quadrality scheme based on category theory and a novel measurement theory were also presented as promising approaches for analyzing the detailed physical properties of DPs, leading to the development of a new field of off-shell science.

The Appendix discusses the spatial resolution and the contrast of the image acquired by a microscope and spectrometer using such a fiber probe.

**References**

[1] H.Sakuma, I. Ojima, and M. Ohtsu: "Dressed photons in a new paradigm of off-shell quantum fields," Progress in Quantum Electronics, **55**, (2017) pp.74-87.

[2] M. Ohtsu (ed.): *Near-Field Nano/Atom Optics and Technology* (Springer, Tokyo, 1998) pp.45-100

[3] Y. Narita, T. Tadokoro, T. Ikeda, T. Saiki, S. Mononobe, and M. Ohtsu: "Near-Field Raman Spectral Measurement of Polydiacetylene," Appl. Spectroscopy, **52** (1998) pp.1141-1144.

[4] M. Ohtsu (ed.): *Near-Field Nano-Optics and Atom Deflection* (Springer, Tokyo, 1998) pp.133-192.

[5] M. Ohtsu: "New Routes to Studying the Dressed Photon," Offshell:1709R.001.v1.

[6] M. Ohtsu and K. Kobayashi: *Optical Near Fields* (Springer, Berlin, 2004) p.23.

[7] T. Yatsui and M. Ohtsu: "High-Throughput Probes for Near-Field Optics and Their Applications," *Prog. Nano-Electro-Optics* (ed. M. Ohtsu) (Springer, Berlin, 2003) p.12.

[8] M. Ohtsu and K. Kobayashi: *Optical Near Fields* (Springer, Berlin, 2004) pp.29-30.

[9] M. Ohtsu, T. Kawazoe, and H. Saigo: "Spatial and Temporal Evolutions of Dressed Photon Energy Transfer," Offshell:1710R.00.v1.

[10] M. Ohtsu: *Dressed Photons* (Springer, Heidelberg, 2014) pp.18-36.

[11] A. Taflove: *Computational Electrodynamics: The Finite-Difference Time-Domain Method* (Artech House, Boston, 1995).

[12] I. Banno and M. Ohtsu, "Irrationality of the Permittivity in Non-resonant Near-field Optics," Abstract of the 11th Asia-Pacific Conference on Near-Field Optics, July 10-13, 2017, Tainan, Taiwan, p.35.

[13] H. Sakuma, I. Ojima, and M. Ohtsu: "Gauge symmetry breaking and emergence of Clebsch-dual electromagnetic field as a model of dressed photons," Appl. Phys. A (2017) 123:750.

[14] I. Ojima: "Micro-macro duality in quantum physics," *Stochastic Analysis: Classical and Quantum Perspectives of White Noise Theory* (ed. T. Hida) (World Scientific, Singapore, 2005) pp.143-161.

[15] O. Bratteli and D.W. Robinson: *Operator Algebras and Quantum Statistical Mechanics* (2nd ed.), vols.1 and 2 (Springer, Berlin, 1987,19977).

**Appendix Spatial resolution and image contrast in measurements using a fiber probe**

As was reviewed in Section 1, DPs have been used in a novel microscope and a spectrometer with ultrahigh spatial resolution beyond the diffraction limit of light. The NPs in Figs. 2(a) and 3(a) correspond to the specimens to be measured by these instruments. In the I-mode, the DP on the tip of the fiber probe serves as a light source to illuminate the specimen. In the C-mode, the light source is the DP on the NP, which is picked up by the fiber probe.

In order to analyze the spatial resolution and contrasts of the acquired microscopic and spectroscopic images, the cross-sectional profile of the fiber probe is shown in Fig. A(a), as was given in Fig. 4(b) [8]. Here, $a_p$ is the tip radius, $d_f$ is the diameter of the foot of the taper protruding from an opaque metallic film, which is deposited for blocking the propagating scattered light, and $\theta$ is the cone angle. The spatial resolution of the measurement is governed by the size of the DP created on the tip, which is equivalent to the tip radius $a_p$, because the spatial profile of the DP field is represented by the Yukawa function.



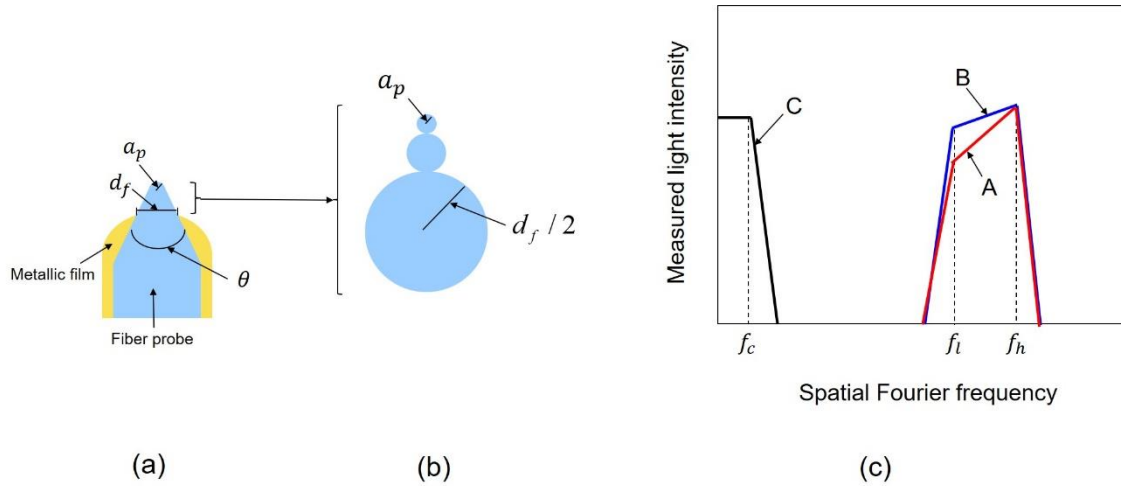(a)                    (b)                    (c)

Fig. A   A fiber probe and spatial Fourier spectra of the acquired image.
(a) Cross-sectional profile of the fiber probe. (b) A taper approximated by a chain of spheres.(c) Spatial Fourier spectrum of the image acquired in the Collection mode. Lines A and B correspond to the fiber probe with small and large cone angles $\theta$, respectively. Line C represents the spectrum acquired by a conventional optical microscope.

Here, the contributions from the DPs created on the taper have to be also considered for evaluating the contrast of the acquired image. For this consideration, Fig. A(b) schematically explains that the taper is approximated as a chain of small spheres which are connected in order to increase the radius, from $a_p$ up to $d_f/2$, as shown in Fig. 10. These spheres receive the DP energy created on the NP in the case of the C-mode, whereas they create the DP on their surfaces in the case of the I-mode. Therefore, in the case of the C-mode, due to the size-dependent resonance feature of the DP energy exchange [10], high-efficiency measurement is achieved if the size of the DP on the NP falls between $a_p$ and $d_f/2$. This means that this efficiency has the characteristics of a spatial band-pass filter. Its spatial Fourier spectra are shown by the lines A and B in Fig. A(c). They show that the C-mode can detect a DP whose size falls within the pass band of this spatial filter (i.e., between $a_p$ and $d_f/2$). Its high-frequency cutoff $f_h$ is proportional to $a_p^{-1}$, showing that the spatial resolution is determined by $a_p$. On the other hand, the low-frequency cutoff $f_l$ is proportional to $d_f^{-1}$.

Figure A(c) shows that with a smaller $e$ (line A), a lower efficiency is exhibited at $f_l$ than that with a larger $e$ (line B), because the sphere of radius $d_f/2$ is farther from the tip in the case of a smaller $e$. This means that the sharper fiber probe can achieve higher selectivity in measuring the DP with a size as small as the tip radius $a_p$. In other words, the high-spatial-resolution component in the image is acquired with higher contrast. In the case of the I-mode, the lines A and B represent the size dependence of the DP energy created on the fiber probe; that is, a DP with a size ranging from $a_p$ to $d_f/2$ is efficiently created.

A conventional optical microscope collects propagating light scattered from the specimen with convex lenses for acquiring an image of the specimen. The spatial Fourier spectrum of the acquired image is represented by the line C in Fig. A(c). Due to the diffraction limit of light, it has the characteristics of a low-pass filter, whose high-frequency cutoff $f_c$ is determined by the wavelength ` of the light, i.e., is

16

proportional to $\grave{\ }^{!1}$.

By comparing the lines A, B, and C, it is confirmed that the spatial resolution of the microscope using DPs is much higher than that of the conventional microscope because $a_p \ll \grave{\ }$ ( $f_h \gg f_c$ ), which is the origin of the name "ultrahigh spatial resolution microscope"

It should be noted here that the spatial Fourier spectral characteristics of the microscopic images acquired by this ultrahigh spatial resolution microscope and the conventional optical microscope do not have any strong correlation between each other. In other words, the images acquired by these microscopes are totally different from each other, in addition to the ultrahigh spatial resolution feature of the former. This is because their spatial filtering characteristics are different; i.e., band-pass filtering and low-pass filtering. By noting the size-dependent resonance feature of the DP energy exchange [10], it should be pointed out that the microscope using DPs acquires an image of the fiber probe tip itself instead of an image of the specimen NP.